ADVANCED FUNCTIONAL MATERIALS
www.afm-journal.de

Molecular Packing-Induced Transition between Ambipolar and Unipolar Behavior in Dithiophene-4,9-dione-Containing Organic Semiconductors

*Huan Xu, Ye-Cheng Zhou, Xing-Yu Zhou, Ke Liu, Lu-Ya Cao, Yong Ai, Zhi-Ping Fan, and Hao-Li Zhang**

By changing the packing motif of the conjugated cores and the thin-film microstructures, unipolar organic semiconductors may be converted into ambipolar materials. A combined experimental and theoretical investigation is conducted on the thin-film organic field-effect transistors (OFETs) of three organic semiconductors that have the same conjugated core structure of s-indaceno[1,2-b:5,6-b′]dithiophene-4,9-dione but with different *n*-alkyl groups. The optical and electrochemical measurements suggest that the three organic semiconductors have very similar energy levels; however, their OFETs exhibit dramatically different transport characteristics. Transistors based on compound 1a or 1c show ambipolar transport properties, while those based on compound 1b show p-type unipolar behavior. Specifically, compound 1c is characterized as a good ambipolar semiconductor with the highest electron mobility of 0.22 $cm^2 V^{-1} s^{-1}$ and the highest hole mobility of 0.03 $cm^2 V^{-1} s^{-1}$. Complementary metal oxide semiconductor (CMOS) inverters incorporated with compound 1c show sharp inversions with high gains above 50. Theoretical investigations reveal that the drastic difference in the transport properties of the three materials is due to the difference in their molecular packing and film microstructures.

1. Introduction

Organic field-effect transistors (OFETs) have attracted much attention in recent years owing to the advantages such as mechanical flexibility and potential low-cost large-area fabrication, leading to possible applications in future electronic devices.[1] The performances of OFETs are largely dependent on the characteristics of the organic semiconductors used as the active layer in the devices. Most OFETs reported so far exhibited unipolar transport properties, *ie.* they showed either hole-transport (p-type) or electron-transport (n-type) properties.[2] Ambipolar OFETs, which allow both electron and hole transports to occur, are attracting increasing interests in recent years due to their potential applications in light-emitting transistors and complementary metal oxide semiconductor (CMOS)-like logic circuits.[3] Much effort is being made to develop suitable materials for ambipolar OFETs.[4] However, in contrast to the large number of p- or n-type materials reported in the literature, much fewer ambipolar organic semiconductors have been studied. Consequently, fundamental understanding on the structure-property relationship of ambipolar materials is still limited.[5]

The performance of an OFET is determined by a number of factors, including the intrinsic electronic structure of the semiconductor, molecular packing, film morphology, dielectric layers, and contact metals, etc.[6] The interconnections between various factors make the correlation between molecular structure and device performance complicated. In a simplified view, that are effectively two basic processes determining the device performance, these are charge injection at the metal/molecule interface and the charge transport within the active layer of the organic semiconductors.[7] Though, many theoretical investigations have indicated that most organic semiconductors are able to transport both hole and electron in their crystals,[8] the majority of OFET devices have only shown unipolar transport behavior, *ie.* only hole or electron transport can be observed. The unipolar behaviors of the OFET devices can be attributed to the fact that the charge injection barriers at the electrode/molecule interface favor the transport of only one type of charge carriers. Under such a condition, the transport properties of organic semiconductors are mostly determined by their energy levels related to the electrode Fermi levels.[9] Large efforts have been made to adjust the molecular energy levels of organic materials to tune their properties. For example, we have reported that by lowering the highest occupied molecular orbital (HOMO) and the lowest unoccupied molecular orbital (LUMO) energy levels, heteropentacene materials can exhibit high and balanced hole and electron transport behaviors.[10] Correlation between the charge transport properties of several organic molecules and their frontier molecular orbital levels have been discussed by

H. Xu, Y.-C. Zhou, X.-Y. Zhou, K. Liu, L.-Y. Cao, Y. Ai, Z.-P. Fan, Prof. H.-L. Zhang
State Key Laboratory of Applied Organic Chemistry (SKLAOC)
College of Chemistry and Chemical Engineering
Lanzhou University
Lanzhou, 730000, PR China
E-mail: Haoli.zhang@lzu.edu.cn

DOI: 10.1002/adfm.201302855

Bao et al.[11] The other fundamental process, the charge transport process, is also crucial to the performance of OFETs. The transport of charge carriers within the active layer of a transistor is strongly influenced by the molecular packing and the thin film structure. Increasing the crystallinity of the active layer by annealing is an efficient way to improve the performance of OFETs.[12] The crystal structure can also affect the device performance. For example, typical p-type material PcCu is known to have different crystal phases, which show different hole mobilities.[13] Park et al. have recently reported a n-type material that have two crystal phases, in which one phase exhibits a higher electron mobility than the other one.[14] To date, the majority of researches suggested that the charge-carrier type of an OFET is mainly determined by the charge injection process; meanwhile, molecular packing appears to affect only the magnitude of the charge mobility but not the type of charge carriers.[15] Indeed, there has not been any experimental work showing that changes in molecular packing can change the charge-carrier type of OFETs.

We report in this work an exceptional case, in which a series of organic semiconductors have the same HOMO/LUMO energy levels exhibited drastically different charge transport properties due to their different molecular packing. A series of s-indaceno [1,2-b:5,6-b′] dithiophene-4,9-dione derivatives containing different alkyl chains were synthesized and fabricated into field effect transistors (**Figure 1**). These molecules have the identical conjugated core, hence very similar electronic energy levels. However, under the same condition, the thin film transistors made from these molecules exhibited either ambipolar or unipolar transport behaviors due to their different molecular packing. The ambipolar material can be used to fabricate CMOS-like inverters with excellent performance.

2. Results and Discussion

2.1. Electronic Structures

The synthesis and basic spectroscopic data of these molecules have been reported in our previous publication.[16] Herein, we only discuss their electronic structures related to their charge transport properties. The UV–vis absorption spectra of their dilute solutions in dichloromethane (DCM) are shown in Figure S1a. As expected, the three molecules exhibit nearly identical absorption bands corresponding to the same conjugate

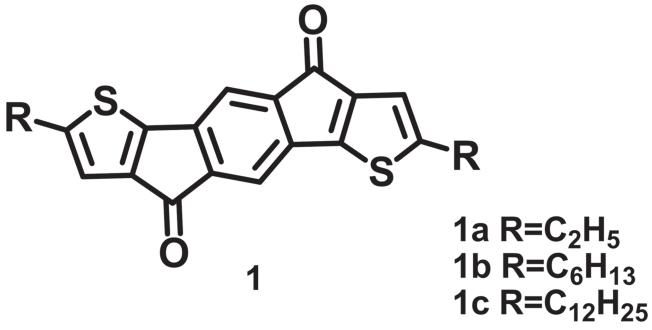

Figure 1. Structures of the compounds **1a–1c.**

Table 1. Optical absorption wavelengths (λ), calculated energy gaps (E_g) and electrochemical properties for the compounds **1a–1c**.

Compounds	λ_{Film} [nm]	λ_{soln} [nm]	$Eg_{(Film)}$ [eV][a)]	$Eg_{(Soln)}$ [eV][a)]	$E^{1/2red}$ [V][b)]	E_{HOMO}/E_{LUMO} [eV][b)]
1a	327, 626	297, 596	1.57	1.70	–0.96	–5.18/–3.48
1b	310, 655	297, 598	1.53	1.72	–0.99	–5.17/–3.45
1c	330, 670	297, 603	1.48	1.71	–1.03	–5.12/–3.41

[a)]Optical HOMO–LUMO gaps were determined from the onset of lowest-energy visible absorption band; [b)]Recorded $E_{1/2}$ values vs. SCE in THF with TBAPF6 as supporting electrolyte. LUMO energies were determined by: $E_{LUMO} = -E_{1/2}^{red} - 4.44$.

core. The thin film spectra show a significant red shift of the absorption edge, suggesting a strong π–π stacking in the solid state. With the lengthening of n-alkyl chains, there is a small reduction of the optical band gaps, but the change is almost neglectable. Cyclic voltammograms (CV) were recorded in tetrahydrofuran (THF) to measure their energy levels (Figure S2). Only reduction peaks have been observed, from which the LUMO levels position were estimated using ferrocene as the reference. The HOMO levels were estimated referring to the LUMO levels and the optical band gaps of the solutions (**Table 1**). Our measurements indicate that these molecules have similar HOMO (ca. –5.1 eV) and LUMO (ca. –3.4 eV) positions. The narrow band gaps suggest that they may exhibit ambipolar behaviors.[3a,10a]

2.2. Film Characterization

In order to compare their transport properties, we have fabricated thin film transistors using these three compounds under identical conditions. The transistors were fabricated using the top contact device structure on octadecyltrimethoxysilane (OTMS) treated Si/SiO_2 substrates. The organic layer was prepared through vacuum deposition at different substrate temperatures (T_{sub}), typically 60 °C to 100 °C. The compound **1a** cannot be deposited into thin film at T_{sub} = 100 °C, probably due to its low thermal stability (it has the lowest weight loss temperature of the three compounds, as shown in thermal gravimetric analysis).[16a] The film morphology of these three compounds deposited on OTMS-Si/SiO_2 substrates at various T_{sub} was investigated by atomic force microscopy (AFM) (**Figure 2**). These materials afford crystalline thin films with lamella-like layered structure on the substrates and the crystal grain size increases with the increase of T_{sub} during the deposition. The morphological improvement at T_{sub} = 80 °C is evident in the multilayer terraces and increased grain sizes, which is expected to enhance the mobility (**Table 2**). At their highest T_{sub}, the films exhibited smoother surface and larger grains comparing with that at lower temperatures. The large grain size may be beneficial for the elimination of the disordering effect and hence provides high mobility. Their good intercrystalline contacts ensure the increase in mobility as well.

The representative OFET characteristics of compounds **1a–1c** are shown in **Figure 3**, and OFET properties obtained at different T_{sub} are summarized in Table 2. It is readily noticed from Table 2 that the three materials exhibited distinctly

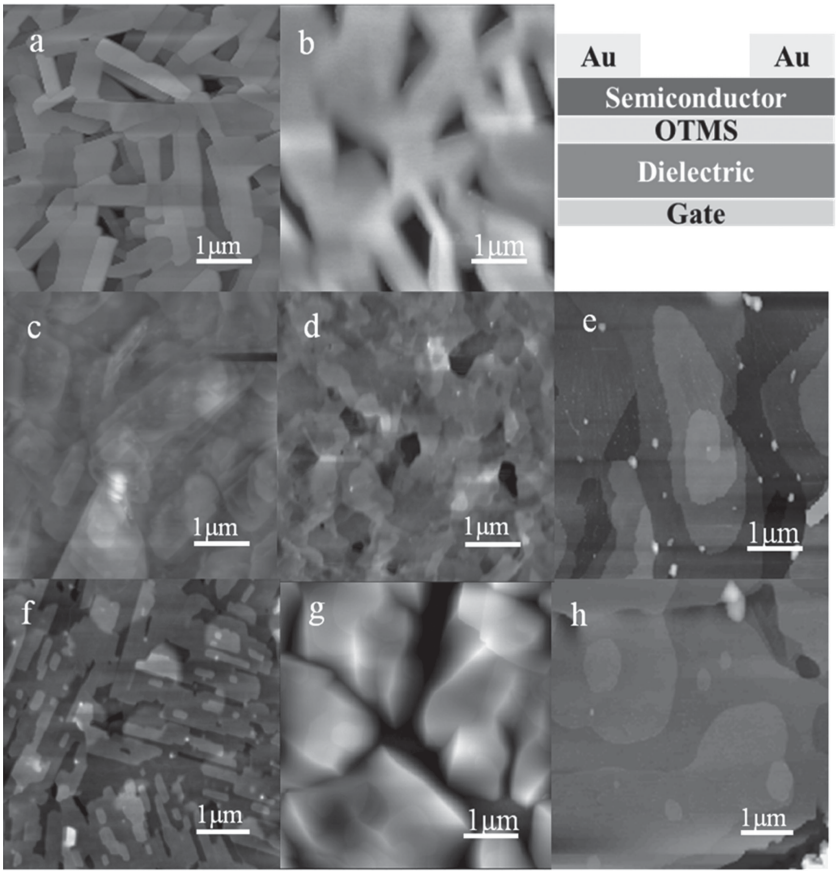

Figure 2. AFM images of the compounds **1a**–**1c** deposited on OTMS-Si/SiO_2 substrates at different temperatures. (a) **1a** at 60 °C, (b) **1a** at 80 °C, (c) **1b** at 60 °C, (d) **1b** at 80 °C, (e) **1b** at 100 °C, (f) **1c** at 60 °C, (g) **1c** at 80 °C and (h) **1c** at 100 °C. The structure diagram of OFET device is shown in the top right corner.

different transport properties. Figure 3a and b show the typical output and transfer curves of **1a** deposited at T_{sub} of 80 °C. Compound **1a** exhibited clearly ambipolar transport properties with the highest electron mobility of 0.043 $cm^2\ V^{-1}\ s^{-1}$ and the highest hole mobility of 0.023 $cm^2\ V^{-1}\ s^{-1}$. In contrast, the compound **1b** exhibited only hole transport properties at different conditions, and no electron transport behavior can be observed (Figure 3c and d). The mobility of **1b** increases with the increase of T_{sub}, and a relatively high mobility of up to 0.05 $cm^2\ V^{-1}\ s^{-1}$ with an on/off ratio of 4×10^3 was obtained at T_{sub} = 100 °C. The good OFET performance at high T_{sub} is attributed to the highly ordered thin film as revealed by the AFM investigations (Figure 2). This unipolar transport property of **1b** is consistent with the observation from Geng's group.[16b] Compound **1c** also exhibited ambipolar transport properties. Figure 3e and f show the typical OFET characteristics of **1c** deposited at T_{sub} of 100 °C. The highest electron and hole mobilities are 0.22 $cm^2\ V^{-1}\ s^{-1}$ and 0.03 $cm^2\ V^{-1}\ s^{-1}$, respectively. Table 2 indicates that the OFET performance of the devices is strongly dependent on the T_{sub} during the deposition. Despite the T_{sub}-induced variation in mobility values, all the transistors from compounds **1a** and **1c** showed ambipolar transport behaviors with their electron mobilities higher than hole mobilities; but devices of the compound **1b** exhibited only unipolar p-type transport properties. As mentioned above, these three molecules have very similar energy levels, and hence the charge injection barriers between the metal Fermi levels to the molecular energy levels should be similar. Therefore, the distinctly different transport behaviors are most likely due to the differences in the charge transport process. To verify this hypothesis, we further investigated the molecular packing of the three molecules in both crystals and thin films.

Table 2. FET characteristics of compounds **1a**–**1c** films deposited on the OTMS-Si/SiO_2 substrates in vacuum at different substrate temperatures. N.O. stands for 'not observed'.

Compounds	T_{sub} [°C]	μ_h [$cm^2\ V^{-1}\ s^{-1}$]	μ_e [$cm^2\ V^{-1}\ s^{-1}$]	on/off ratio	V_T [V]
1a	60	6.9×10^{-4}	0.030	$3 \times 10^2/3 \times 10^4$	–71/47
	80	0.023	0.043	$3 \times 10^3/2 \times 10^4$	–47/23
1b	60	0.005	N.O.	5×10^2	–55
	80	0.02	N.O.	1×10^3	–75
	100	0.05	N.O.	4×10^4	–26
1c	60	0.007	0.02	$2 \times 10^2/1 \times 10^2$	–8/43
	80	0.03	0.10	$2 \times 10^4/2 \times 10^4$	–14/40
	100	0.02	0.22	$5 \times 10^3/1 \times 10^4$	–22/40

2.3. Single Crystal Structures

Single crystals of compounds **1a**–**1c** were prepared by slow evaporation of solution from a chloroform/ethanol mixture. Compounds **1a**–**1c** all crystallize in triclinic crystal system with *P*-1 space group. The main five-ring-fused backbone shows planar structure in all the three crystals, while the n-alkyl chains on the α-position of thienyl groups lie outside of the skeleton plane (**Figure 4**). All the three compounds form slipped face-to-face π-stacking motifs in the crystals. A layer-by-layer structure is formed along the *c* axis without the interdigitation of alkyl chains. This type of molecular arrangement is expected to give a stronger electronic coupling between the molecules than the herringbone arrangement. The π–π stacking interplanar distances for **1a**, **1b** and **1c** are 3.55 Å, 3.25 Å and 3.49 Å, respectively. Weak C–H···O hydrogen bonds can be found in the three crystals. As shown in Figure 4a, in the crystal of **1a**, the H···O distances are 2.56 Å and 2.58 Å, which exist between the carbonyl groups and the H atoms of the ethyl groups in another layer. For **1b**, hydrogen bonds are formed in the same layer between the carbonyl groups and the H atoms on the thiophene rings

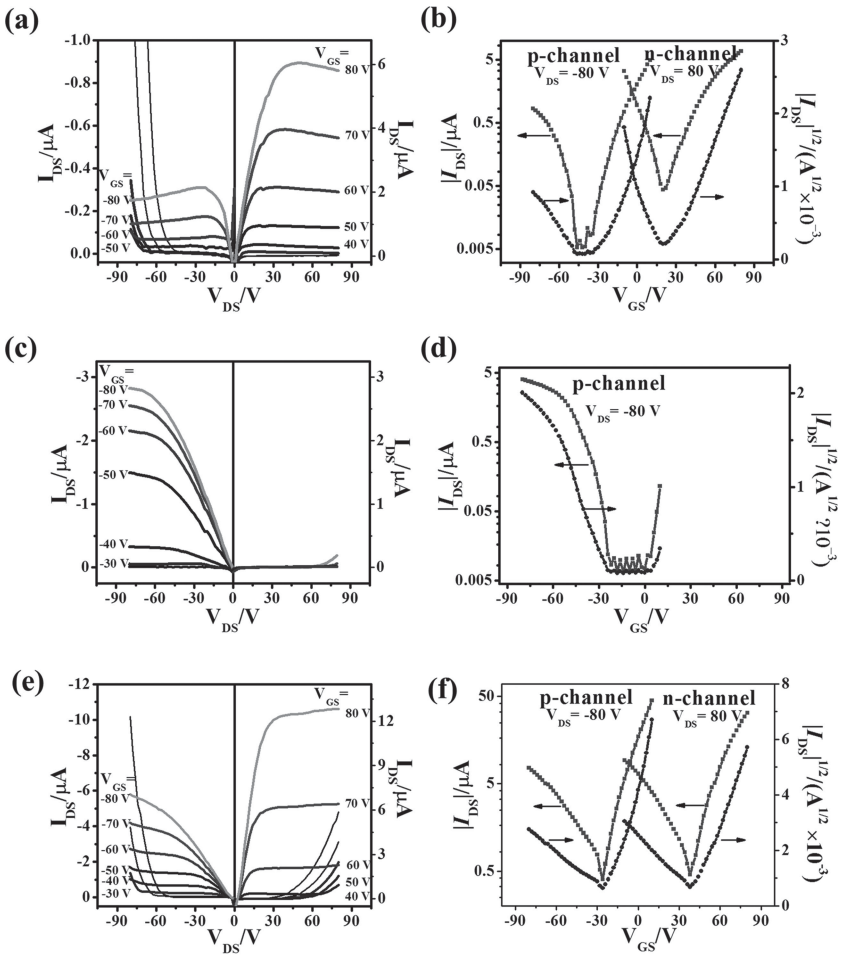

Figure 3. Typical output (left) and transfer (right) curves of compounds **1a**–**1c** deposited on the OTMS-Si/SiO_2 substrates. (a,b) **1a** with T_{sub} = 80 °C, (c,d) **1b** with T_{sub} = 100 °C, and (e,f) **1c** with T_{sub} = 100 °C.

(indicated as I and II in Figure 4a), and the H···O distance is 2.51 Å. For **1c**, the H···O distance is 2.43 Å between the carbonyl groups and the H atoms on the benzene rings in the neighboring layer. Remarkably, marked S···O short contacts (3.12 Å) were found between the neighboring columns of **1c**. The strong intraplanar S···O interactions link the columns into layered structures. Bao[17] and Zhu[18] have reported that such a double-channel fashion of molecular packing may facilitate carrier transport and result in high device performance, which may explain the high electron mobility of **1c** at T_{sub} = 100 °C.

Particularly, the interplanar distance (3.25 Å) of **1b** is shorter than the corresponding values of **1a** and **1c** in the same layer (shown in Figure 4c). However, the intermolecular π–π overlap of **1b** is less than the other two due to the larger transverse shift (more than half molecular width) between the molecules in the adjacent molecular layers (I and III in Figure 4b). Whereas in the crystals of **1a** and **1c** (Figure 4a and c), much larger molecule overlapping occurred between the two adjacent layers. The different degree of molecular overlapping in the three crystals implies different intermolecular coupling, which is expected to have significant impact on their charge mobilities.[3a,6d]

2.4. X-Ray Diffraction Measurements

Because the transistors were fabricated using the thin films of the compounds, it is necessary

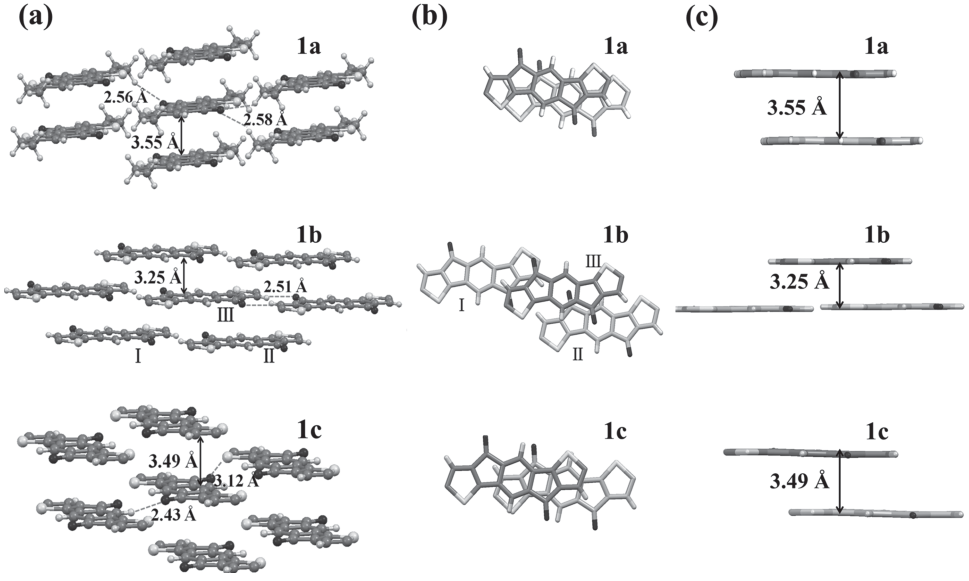

Figure 4. Crystal structures of the compounds **1a**–**1c**. The solid lines outline the π–π stacking distances, and the dash lines outline the C–H···O and S···O interactions between the molecules. The alkyl chains are omitted for clarity. (a) The packing diagrams of **1a**–**1c**, (b) the top view of the crystal structures, and (c) the side view of the crystal structures.

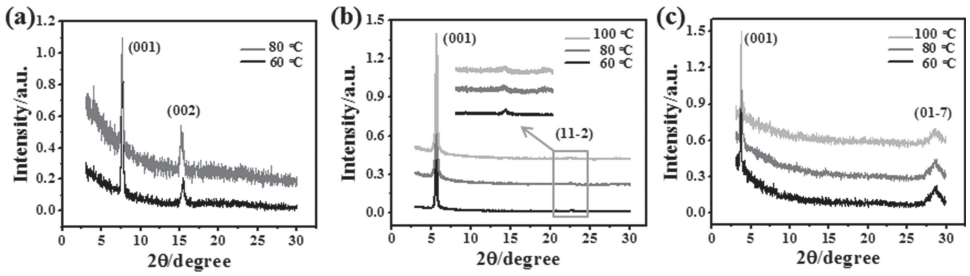

Figure 5. X-Ray diffraction patterns of the thin films of the compounds (a) **1a**, (b) **1b**, and (c) **1c** deposited on the OTMS-Si/SiO_2 substrates at different temperatures.

to investigate the crystallinity and the orientation of the three molecules in their thin films.[19] X-Ray diffraction (XRD) measurements were performed on the thin films deposited on OTMS-Si/SiO_2 substrates at various T_{sub} (**Figure 5**). The XRD patterns were analyzed by using the Mercury software. For the compound **1a**, two peaks were observed (Figure 5a). These are the stronger peak at 7.61° related to a *d*-spacing of 11.60 Å and the weaker peak at 15.25° related to a *d*-spacing of 5.80 Å corresponding to the (001) and (002) planes of the single crystal. The *d*-spacing of 11.60 Å of the first peak in the thin film is close to the unit-cell parameter *c* of the single crystal (12.30 Å). Therefore, the *c*-axe of **1a** in the thin films orient 87.7° with respect to the substrate surfaces, while *a* and *b* axes are arranged in the plane. The molecules contact the substrate via their alkyl chains and exhibit a layer-by-layer packing on the substrate, while the long axis of the conjugated core has an angle of 59.9° with respect to the substrate.

While for the compound **1b**, the distinct peak at 5.64° corresponds to a *d*-spacing of 15.65 Å, close to the unit-cell parameter *c* of the single crystal 15.80 Å, which can be assigned to the (001) plane. The *c*-axe of **1b** in the thin films orient 82.1° with respect to the substrate surfaces, while *a* and *b* axes are arranged in the plane. The molecule exhibits layer-by-layer packing on the substrate and the angle with respect to the substrate is 72.5°. Another weak peak was observed at 22.34° related to a *d*-spacing of 3.98 Å, which is assigned to the (11–2) plane (Figure 5d). It indicates that there is a second crystalline phase in the thin films. In the crystalline (11–2) cryatallite, the *c*-axe of **1b** orients 33.4° with respect to the substrate surfaces. The long axis of the conjugated core has an angle of 56.2° with respect to the substrate (**Figure 6**d).

Figure 5c shows that two diffraction peaks were observed for the thin film of compound **1c**. The stronger peak at 3.69° corresponds to a *d*-spacing of 23.9 Å, close to the unit-cell parameter *c* of the single crystal 24.3 Å, which can be assigned to the (001) plane. The weaker peak at 28.18°, corresponding to a *d*-spacing of 3.16 Å, is assigned to the (01–7) plane. Similar

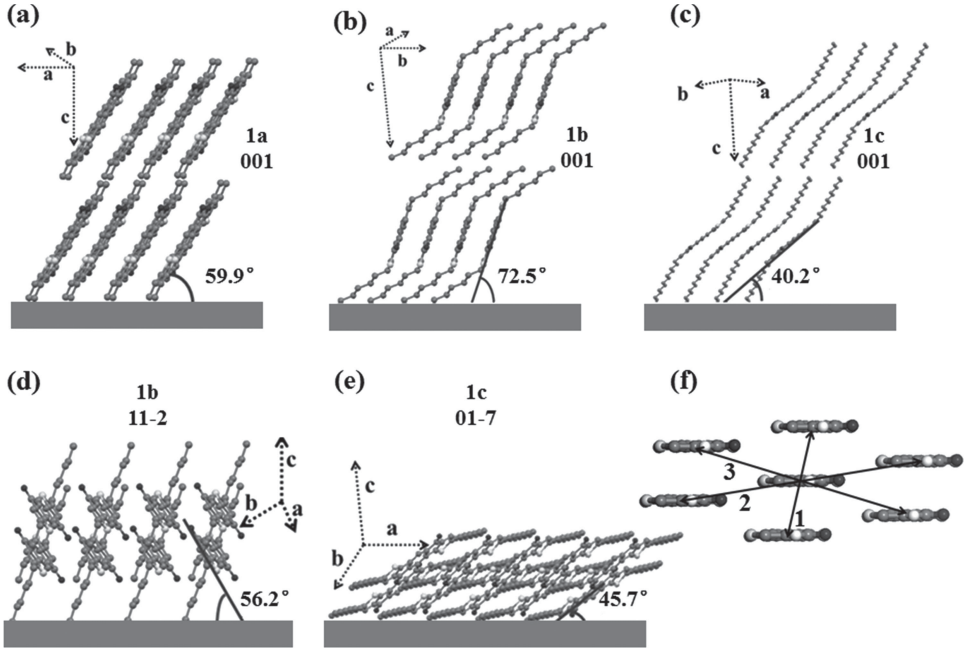

Figure 6. The molecular packing of compounds (a) **1a**, (b) **1b** and (c) **1c** in their (001) crystalline grain; (d) molecular packing of **1b** in its (11–2) crystalline grain; (e) molecular packing of **1c** in its (01–7) crystalline grain; (f) charge hopping pathway scheme for **1a**–**1c** (they have similar charge hopping pathway).

to that of the **1b**, there are also two crystalline phases in the thin films of **1c**. For the (001) plane, the *c*-axe of **1c** in the thin films orient 79.6° with respect to the substrate surfaces, while *a* and *b* axes are arranged in the plane. The molecules exhibit a layer-by-layer packing on the substrate with the long axis of the conjugated core has an angle of 40.2° with respect to the substrate (Figure 6c). For the (01–7) plane, the *c*-axe of **1c** in the thin films orient 61.7° with respect to the substrate surfaces, and the angle between the long axis of the conjugated core and the substrate is 45.7° (Figure 6e).

2.5. Theoretical Analysis

The transport properties of a transistor can be affected by a variety of factors, including thin film morphologies, reorganization energies, intermolecular orbital overlap, interface dipoles, and charge traps. The above characterization has shown that the three compounds **1a–1c** have very similar electronic structures and similar film morphology, except that they show different molecular packing motif in their single crystals and different XRD patterns of their thin films. Trap is an important factor that could affect the charge transport properties. The traps at the molecule/dielectric interface are particularly important because they affect directly the charge transport channel. For example, previous work have shown that the the SiO_2 dielectric layer presents a large number of hydroxyl groups on its surface, which act as traps for electrons. To allow electron transport to be observed, the traps at the SiO_2 layer surface must be removed.[6d,20] Furthermore, in a FET device, not all induced charges are mobile and contribute to the transport. Deep traps first have to be filled before the additionally induced charges become mobile, so that traps are expected to have significant effects on the threshold voltages.[3a] In this work, the SiO_2 surface was treated by octadecyltrimethoxysilane (OTMS) under the same condition. Though not all the traps can be removed, it is reasonable to assume that the trap densities are similar in the devices prepared from the three materials, so that the observed differences in the transport properties should be mainly determined by their intrinsic molecules properties, but less related to the device fabrications conditions. Assuming that the interface dipoles, and charge traps are essentially constant for the present molecules due to molecular structure/device similarities, the differences in their FET performances can be mainly attributed to their different molecular packing and thin film structures.

Brédas et al.[6d,21] have used quantum chemical calculation to discuss how the amplitude of the transfer integrals is influenced by various aspects of molecular packing. They have shown that the configuration of molecules in their crystals can affect the mobilities for electrons and holes. Meanwhile, Shuai et al.[22] have investigated the influences of crystal packing, molecule size, orbital coupling on the hole mobility of oligothiophenes. Accordingly, we then investigated the effects of molecular packing on the hole and electron mobilities using theoretical simulation. We have calculated the theoretical mobilities of the different crystals following the protocols established by Brédas,[6d,21] Shuai[22,23] and Deng et al.[24]

Briefly, in our calculation, carrier movement in the organic material was viewed as a result of series hopping between the neighboring molecules. The hopping rate can be described by the Fermi golden rule.[25] The electronic coupling strength between two nearby molecules is described by the effective transfer integral (*V*), which is obtained by the site-energy correction method.[26] In order to take into account the effects of thermal fluctuations during the hopping events, a molecular dynamics (MD) simulation was performed to obtain the Gaussian distribution in energy. Then Kinetic Monte Carlo processes were performed to obtain the diffusion coefficient (D), which enables the calculation of mobilities via the Einstein relation:

$$\mu = \frac{eD}{k_B T} \tag{1}$$

More details of the simulation procedure and the calculated reorganization energies are available in the Supporting Information.

As indicated by the XRD data, all the three molecules form layered structure on the substrates (Figure 6 and Figure S3). Figure S3 illustrate the in-plane molecular packing of the three molecules based on their crystal structures, from which the electronic coupling between the neighboring molecules can be calculated. Within one layer, each molecule has six nearest neighbors. From the symmetry, we only need to consider the electronic coupling for three typical molecular pairs, labeled as 1, 2, and 3 in Figure 6f. Each molecular pair represents one possible electron hopping pathway. The electronic coupling (*V*) of the three molecular pairs in each crystal can then be calculated using the method described above, and the results are listed in **Table 3**. The calculated *V* of the different molecular pairs provides information on the overall intermolecular electronic coupling strength, which could be then used to estimate the theoretical mobilities in the crystals.[24a] However, it should be kept in mind that the molecular packing in the thin films is different from that in their crystals. Therefore, the calculation must correlate to the specific molecular packing in the thin films of each molecule.

Table 3. The distances (d), mean values of electronic coupling (V^2) and theoretical diffusion mobilities $\mu_{(cal.)}$ ($cm^2\ V^{-1}\ s^{-1}$) at room temperature (300 K) for all pathways of **1a**, **1b** and **1c**.

Molecules	Pair[a)]	d [Å]	V_e^2	$\mu_{e\ (cal.)}$	V_h^2	$\mu_{h\ (cal.)}$
1a	1	4.10	12397	3.93[b)]	10861	3.47[b)]
	2	8.40	717.99		19.31	
	3	8.69	8.08		1.2	
1b	1	5.11	6118.9	5.20[b)]	2525.8	2.46[b)]
	2	11.33	21.36		0.66	
	3	8.31	288.13	0.20[c)]	1382.2	2.00[c)]
1c	1	5.50	759.78	5.12[b)]	10719	6.49[b)]
	2	7.07	63.72	0.04[d)]	5.07	0.01[d)]
	3	7.64	392.71		2.74	

[a)]Molecular pairs as shown in Figure 6f; [b)] Calculative mobility of (001) crystalline grain based on a random walk hopping process; [c)]Calculative mobility of the thin film assuming pair 3 plays dominating role in the hopping process; [d)]Calculative mobility of the thin film assuming pair 2 plays dominating role in the hopping process.

Figure 5 shows that all the films exhibit strong (001) peaks. Comparing the calculated *d*-spacing values with the molecular lengths, we have concluded that the molecules were deposited on the substrates into layer-by-layer stacks with their long axes oriented nearly perpendicular to the substrates in their (001) crystalline grains (Figure 6a–c). Compound **1a** shows a (002) peak in the XRD pattern with no other diffraction peak, suggesting single type of molecular orientation and highly ordered interlayer spacing (Figure S4). A weak peak corresponding to the (11–2) planes and a prominent (01–7) peak were observed in the thin film of **1b** and **1c**, respectively, indicating coexistence of other crystalline grains in the thin film of **1b** and **1c** (Figure 6d–e).

As mentioned above, the mobilities can be estimated based on the electronic coupling strength. In general, a strong electronic coupling between a given pair corresponds to a high charge transfer rate and consequently high mobility. Table 3 shows the electronic coupling strength (in V^2) of different molecular pairs. Now the question becomes how to properly estimate the mobilities from the calculated *V*. For the thin film of **1a**, the molecules are packed into laminar structure with (001) plane parallel to the charge transport orientations. As the (001) plane favors the in-plane charge transport, therefore, its electron and hole mobilities can be simulated based on a random walk process taking into account of all the three hopping paths. The simulation gives a theoretical electron mobility of 3.93 $cm^2\ V^{-1}\ s^{-1}$ and a theoretical hole mobility of 3.47 $cm^2\ V^{-1}\ s^{-1}$, indicating an ambipolar transport property with electron mobility slightly higher than the hole mobility. The theoretical simulation result is in good agreement with the experimental observation that the FET devices of **1a** exhibit ambipolar transport properties with the electron mobility higher than the hole mobility. Comparing with the best experimental mobilities obtained at T_{sub} = 80 °C (Table 2), the simulation obviously overestimates the mobilities, which can be attributed to the fact the molecular packing in thin films is less ordered than that in the single crystal.

For the thin films of **1b** and **1c**, the situation is more complicated because there are two types of crystalline grains coexisting in the thin films. Li et al. have recently studied the thin film transistors of an anthradithiophene derivative, using microbeam grazing incidence wide-angle X-ray scattering (μGIWAXS).[27] The molecule can form both (001) and (111) crystalline grains, in which the the (001) crystallites have efficient in-plane charge transport but the in–plane charge transport is not efficient in (111) crystallites. They have suggested that the grain does not favor in-plane carrier transport may dominate the carrier transport through a "bottleneck" effect. We believe that the similar phenomena occurred in the thin films of **1b** and **1c**.

For the thin film of **1b**, as XRD data indicating polymorph structure consisting (001) and (11–2) planes, so that both types of molecular packing should be taken into account. The (001) crystallites form π-stacking sheets in the plane of the substrate that favors in-plane charge transport.[27,28] The theoretically calculated mobilities of **1b** in its (001) plane are shown in the Table 3, suggest that **1b** favors electron transport more than hole transport. The theoretical mobilities are 5.20 $cm^2\ V^{-1}\ s^{-1}$ and 2.46 $cm^2\ V^{-1}\ s^{-1}$, for electron and hole, respectively. However, as shown in Figure 3, we have only observed hole transport behavior in the OFET of **1b**. The discrepancy between the simulation and the experiment results indicated that the thin film mobility of the **1b** is not dominated by the (001) crystalline grain. As suggested by Li et al., the grain does not favor in-plane carrier transport may dominate the carrier transport through "bottleneck" effect.[27] In the (11–2) plane, the **1b** molecules do not form strong π-stacking in the plane parallel to the substrate plane, so that the contributions of the three pathways to in-plane carrier transport are different. Figure S5 analyzes the three major hopping pathways with respect to the (11–2) plane. It shows that the hopping pathways along the pair 3 has the largest contribution to the in-plane transport, therefore should have the strongest effect to the charge transport of the (11–2) crystalline grain. Table 3 shows that the electronic coupling (V^2) of pair 3 is much lower than the hole coupling, suggesting much lower electron mobilities than the hole mobilities in the (11–2) crystalline grain, which explains the experimental observation that the OFETs of the **1b** exhibit only a relatively high hole mobility but no electron mobility.

For molecule **1c**, the XRD suggests that its thin films consist of (001) and (01–7) crystalline phases. The (001) crystallites form π-stacking sheets in the plane of the substrate that favors in-plane charge transport.[27,28] The theoretical simulation to the charge transport of the **1c** in its (001) plane give electron mobility of 5.12 $cm^2\ V^{-1}\ s^{-1}$ and hole mobility of 6.49 $cm^2\ V^{-1}\ s^{-1}$. This result suggests that the (001) crystalline grain favors hole transport more than electron transport, which is not consistent to the experimental results. We then analyzed the electon hopping pathways with respect to the (01–7) plane of the **1c**. It is found that the both pair 2 and 3 have large contribution to the in-plane charge transport within the (01–7) crystalline grain (Figure S6). As pair 2 has smaller intermolecular distance, therefore should play a more important role to the mobility. Our calculation to the transfer integral suggests that both pair 2 and 3 have electron coupling higher than the hole coupling, hence a higher electron mobility is expected. This result is qualitatively consistent with the experimental result that the OFETs of **1c** exhibit electron mobility much higher than the hole mobility.

It is very complicated to simulate the transport properties of the thin films consisting two crystalline grains. To provide a reasonable estimation to the carrier mobilities of the thin films of **1b** and **1c**, we have tried to calculate their hole and electron mobilities based on the assumption that the pair 3 in **1b** and pair 2 in **1c** dominate their charge transport. As it is impossible to quantitatively determine the contribution of the different hopping pathways, we have arbitrarily assigned the probability of charge transport through the dominating molecular pairs, i.e., pair 3 in **1b** and pair 2 in **1c**, to be 1000 times higher than that of the other pairs. And the calculated mobilities are shown in Table 3. Although the simulation can not quantatively predict the hole and electron mobilities of the given devices, but the analysis on the possible charge transport pathways in the (11–2) plane of **1b** and (01–7) plane of **1c** gives qualitatively consistent result to the experimental observations and helps to understand their different transport behaviors. More sophisticated characterization and simulation tools are needed for

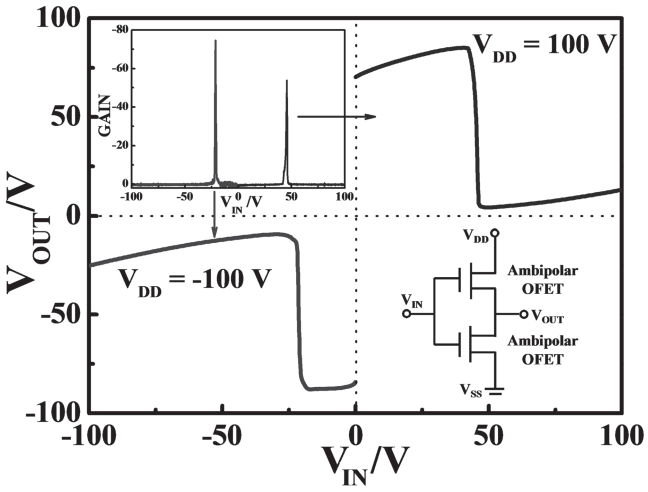

Figure 7. Transfer characteristics of a CMOS-like inverter at V_{DD} of ± 100 V. The circuit configuration is given in the bottom right inset and gain characteristic in the top left inset.

more quantitative analysis to the charge transport within the thin films. After all, the above analysis has suggested that the different transport behaviors of the transistors fabricated using the three molecules are determined by their different molecular packing and microstructures of the thin films.

2.6. Inverter Properties

One important application for amibipolar OFETs is to construct CMOS-like inverters. As both electron and hole can be transported in ambipolar OFET, there is no need to pattern n- and p- type materials into specific areas, the structure of inverters can be much simpler than those based on unipolar FETs. Because the transistor of compound **1c** gives a reasonably high hole mobility and the highest electron mobility among the three materials, we have fabricated an inverter circuit using **1c** by combining two identical OFETs with a common gate as the input voltage (V_{IN}) and a common drain as the output voltage (V_{OUT}). In **Figure 7**, a typical input/output characteristics is shown for an inverter based on two transistors with channel length L = 150 mm and channel width W = 3000 mm. In contrast to the conventional inverters fabricated using unipolar materials, the inverters fabricated by ambipolar transistors work in both negative and positive supply biases.[3a] As expected for an ambipolar inverter, Figure 7 shows that sharp voltage inversion is demonstrated for both negative and positive supply voltages (V_{DD}). For V_{DD} = ±100 V, the highest gains were both higher than 50. Because the hole and electron transport properties are not ideally balanced, the input/output characteristic shows asymmetric characteristic. Under positive bias condition, the voltage inversion takes place at +48 V; while under negative bias, the inversion occurs at -24 V. These results also confirm that compound **1c** is indeed an ambipolar organic semiconductor.

3. Conclusions

Our experimental and theoretical investigations on the field effect transistor properties of the three organic semiconductors have revealed that molecular packing and microstructures of the solid thin films strongly affect their charge transport properties. Though the three semiconductors have the same conjugated core, i.e. similar HOMO and LUMO levels, their different *n*-alkyl substitutes induce changes between ambipolar to unipolar transport behaviors. Compound **1c** exhibits good ambipolar transport properties and can be applied to fabricate CMOS-like inverters with good performance. XRD results suggested that the three molecules form different microstructure in their thin films. Theoretical investigation revealed that the drastic differences in transport properties are due to their different molecular packing and orientations in the thin films induced by the different alkyl substitutes. To our knowledge, this is the first experimental work showing that by tuning the molecular packing and thin film microstructure, unipolar organic semiconductor can be converted into ambipolar materials. It is possible that many previously known unipolar organic semiconductors can also be turned into ambipolar organic semiconductors, and vice versa, by adjusting their molecular packing in OFETs. This finding opens a new venue to search for new ambipolar organic semiconductors for future organic electronics.

4. Experimental Section

General Procedures and Methods: Compounds **1a-1c** were prepared according to our previous publication, where the basic spectroscopic properties of these molecules have also been reported.[16a] UV–vis absorption spectra were measured using a T6 UV–vis spectrometer. CV was run on a CHI660C electrochemistry station (CHI, USA) in 0.1 M Bu_4NBF_4/THF solution. Single crystal date collection was made on a Bruker X8 APEX diffractometer with graphite monochromated Mo–Kα radiation. AFM studies were performed with Agilent 5500. The X-ray diffraction data were obtained at X'Pert PRO made by Panalytical Company with a wavelength of 1.5406 Å.

Device Fabrication: The top-contact/bottom gate devices were made by thermally depositing the molecules onto OTMS-modified SiO_2/Si substrates with 400 nm SiO_2 as the dielectric layer (C_i = 9.0 nF·cm^{-2}). The materials were purified by chromatography on silica gel, recrystallized twice in n-hexane/chloroform mixture solvents. The thin films were deposited at an initial rate of 0.1 Å/s under a pressure of about 4.0×10^{-4} Pa to a final thickness of 20~25 nm as determined by a quartz crystal monitor. The substrate was held at different temperatures during the deposition of the organic layer. Metal electrodes (40 nm) were then fabricated onto the organic layer by evaporation through a shadow mask. The channel width (W) and the channel length (L) were 3000 μm and 150 μm, respectively. OFET properties were measured in both the air and glove box at room temperature with a Keithley 4200–SCS semiconductor characterization system.

[Crystallographic data (excluding structure factors) for the structures reported in this paper have been deposited with the Cambridge Crystallographic Data Centre as supplementary publication no. CCDC 939479 for **1a**, CCDC 751385 for **1b** and CCDC-751386 for **1c**].

Supporting Information

Supporting Information is available from the Wiley Online Library or from the author.

Acknowledgments

This work is supported by National Basic Research Program of China (973 Program) No.2012CB933102, National Natural Science Foundation of China (NSFC. 21233001, 21190034,21073079, J1103307), Specialized Research Fund for the Doctoral Program of Higher Education (SRFDP. 20110211130001) and the 111 Project.

Received: August 14, 2013
Revised: November 26, 2013
Published online: January 23, 2014

[1] a) V. C. Sundar, J. Zaumseil, V. Podzorov, E. Menard, R. L. Willett, T. Someya, M. E. Gershenson, J. A. Rogers, *Science* **2004**, *303*, 1644; b) M. Mas-Torrent, C. Rovira, *Chem. Soc. Rev.* **2008**, *37*, 827; c) Y. Wen, Y. Liu, Y. Guo, Gui Yu, W. Hu, *Chem. Rev.* **2011**, *111*, 3358; d) J. Mei, Y. Diao, A. L. Appleton, L. Fang, Z. Bao, *J. Am. Chem. Soc.* **2013**, *135*, 6724.

[2] a) Y. Wen, Y. Liu, *Adv. Mater.* **2010**, *22*, 1331; b) C. Wang, H. Dong, W. Hu, Y. Liu, D. Zhu, *Chem. Rev.* **2012**, *112*, 2208.

[3] a) J. Zaumseil, H. Sirringhaus, *Chem. Rev.* **2007**, *107*, 1296; b) K.-J. Baeg, J. Kim, D. Khim, M. Caironi, D.-Y. Kim, I.-K. You, J. R. Quinn, A. Facchetti, Y.-Y. Noh, *ACS Appl. Mater. Interfaces* **2011**, *3*, 3205; c) M. Irimia-Vladu, E. D. Głowacki, P. A. Troshin, G. Schwabegger, L. Leonat, D. K. Susarova, O. Krystal, M. Ullah, Y. Kanbur, M. A. Bodea, V. F. Razumov, H. Sitter, S. Bauer, N. S. Sariciftci, *Adv. Mater.* **2012**, *24*, 375.

[4] a) Z. Liang, Q. Tang, R. Mao, D. Liu, J. Xu, Q. Miao, *Adv. Mater.* **2011**, *23*, 5514; b) H. Usta, A. Facchetti, T. J. Marks, *J. Am. Chem. Soc.* **2008**, *130*, 8580.

[5] a) J. Cornil, J.-L. Brédas, J. Zaumseil, H. Sirringhaus, *Adv. Mater.* **2007**, *19*, 1791; b) H. Jiang, *Macromol. Rapid. Commun.* **2010**, *31*, 2007.

[6] a) S. Seo, B.-N. Park, P. G. Evans, *Appl. Phys. Lett.* **2006**, *88*, 232114; b) T. Takahashi, T. Takenobu, J. Takeya, Y. Iwasa, *Appl. Phys. Lett.* **2006**, *88*, 033505; c) E. M. Muller, J. A. Marohn, *Adv. Mater.* **2005**, *17*, 1410; d) V. Coropceanu, J. Cornil, D. A. da Silva Filho, Y. Olivier, R. Silbey, J.-L. Brédas, *Chem. Rev.* **2007**, *107*, 926; e) C. Reese, M. E. Roberts, S. R. Parkin, Z. Bao, *Adv. Mater.* **2009**, *21*, 3678; f) T. Minari, Y. Miyata, M. Terayama, T. Nemoto, T. Nishinaga, K. Komatsu, S. Isoda, *Appl. Phys. Lett.* **2006**, *88*, 083514.

[7] a) J. J. Brondijk, F. Torricelli, E. C. P. Smits, P. W. M. Bloma, D. M. d. Leeuw, *Org. Electron.* **2012**, *13*, 1526; b) B. B.Y. Hsu, E. B. Namdas, J. D. Yuen, S. Cho, D. W. Samuel, A. J. Heeger, *Adv. Mater.* **2010**, *22*, 4649.

[8] a) A. Fuchs, T. Steinbrecher, M. S. Mommer, Y. Nagata, M. Elstnerb, C. Lennartz, *Phys. Chem. Chem. Phys.* **2012**, *14*, 4259; b) J. J. Kwiatkowski, J. Nelson, H. Li, J. L. Brédas, W. Wenzelc, C. Lennartzd, *Phys. Chem. Chem. Phys.* **2008**, *10*, 1852; c) H. Liu, S. Kang, J. Y. Lee, *J. Phys. Chem. B* **2011**, *115*, 5113.

[9] a) F.-C. Chen, L.-J. Kung, T.-H. Chen, Y.-S. Lin, *Appl. Phys. Lett.* **2007**, *90*, 073504; b) C. Di, G. Yu, Y. Liu, Y. Guo, Y. Wang, W. Wu, D. Zhu, *Adv. Mater.* **2008**, *20*, 1286.

[10] a) Y.-Y. Liu, C.-L. Song, W.-J. Zeng, K.-G. Zhou, Z.-F. Shi, C.-B. Ma, F. Yang, H.-L. Zhang, X. Gong, *J. Am. Chem. Soc.* **2010**, *132*, 16349; b) C.-L. Song, C.-B. Ma, F. Yang, W.-J. Zeng, H.-L. Zhang, X. Gong, *Org. Lett.* **2011**, *13*, 2880; c) J. Wang, K. Liu, Y.-Y. Liu, C.-L. Song, Z.-F. Shi, J.-B. Peng, H.-L. Zhang, X.-P. Cao, *Org. Lett.* **2009**, *11*, 2563; d) W.-J. Zeng, X.-Y. Zhou, X.-J. Pan, C.-L. Song, H.-L. Zhang, *AIP Advances* **2013**, *3*, 012101.

[11] M. L. Tang, A. D. Reichardt, P. Wei, Z. Bao, *J. Am. Chem. Soc.* **2009**, *131*, 5264.

[12] a) C. Piliego, D. Jarzab, G. Gigli, Z. Chen, A. Facchetti, M. A. Loi, *Adv. Mater.* **2009**, *21*, 1573; b) A. C. Arias, J. D. MacKenzie, I. McCulloch, J. Rivnay, A. Salleo, *Chem. Rev.* **2010**, *110*, 3.

[13] K. Xiao, R. Li, J. Tao, E. A. Payzant, I. N. Ivanov, A. A. Puretzky, W. Hu, D. B. Geohegan, *Adv. Funct. Mater.* **2009**, *19*, 3776.

[14] S. K. Park, J. H. Kim, S.-J. Yoon, O. K. Kwon, B.-K. An, S. Y. Park, *Chem. Mater.* **2012**, *24*, 3263.

[15] a) T. Lei, Y. Cao, X. Zhou, Y. Peng, J. Bian, J. Pei, *Chem. Mater.* **2012**, *24*, 1762; b) T. Lei, J.-H. Dou, J. Pei, *Adv. Mater.* **2012**, *24*, 6457; c) F. Zhang, Y. Hu, T. Schuettfort, C. Di, X. Gao, C. R. McNeill, L. Thomsen, S. C. B. Mannsfeld, W. Yuan, H. Sirringhaus, D. Zhu, *J. Am. Chem. Soc.* **2013**, *135*, 2338.

[16] a) J. Wang, W. Zeng, H. Xu, B. Li, X. Cao, H. Zhang, *Chin. J. Chem.* **2012**, *30*, 681; b) H. Tian, Y. Deng, F. Pan, L. Huang, D. Yan, Y. Geng, F. Wanga, *J. Mater. Chem.* **2010**, *20*, 7998.

[17] A. L. Briseno, Q. Miao, M.-M. Ling, C. Reese, H. Meng, Z. Bao, F. Wudl, *J. Am. Chem. Soc.* **2006**, *128*, 15576.

[18] a) Y. Sun, L. Tan, S. Jiang, H. Qian, Z. Wang, D. Yan, C. Di, Y. Wang, W. Wu, G. Yu, S. Yan, C. Wang, W. Hu, Y. Liu, D. Zhu, *J. Am. Chem. Soc.* **2007**, *129*, 1882; b) C. Di, G. Yu, Y. Liu, D. Zhu, *J. Phy. Chem. B* **2007**, *111*, 14083.

[19] S. C. B. Mannsfeld, M. L. Tang, Z. Bao, *Adv. Mater.* **2011**, *23*, 127.

[20] L.-L. Chua, J. Zaumseil, J.-F. Chang, E. C.-W. Ou, P. K.-H. Ho, H. Sirringhaus, R. H. Friend, *Nature* **2005**, *434*, 194.

[21] J. L. Brédas, J. P. Calbert, D. A. da Silva Filho, J. Cornil, *Proc. Natl. Acad. Sci. USA* **2002**, *99*, 5804.

[22] X. Yang, L. Wang, C. Wang, W. Long, Z. Shuai, *Chem. Mater.* **2008**, *20*, 3205.

[23] a) L. Wang, Q. Li, Z. Shuai, L. Chenc, Q. Shic, *Phys. Chem. Chem. Phys.* **2010**, *12*, 3309; b) G. Nan, X. Yang, L. Wang, Z. Shuai, Y. Zhao, *Phys. Rev. B* **2009**, *79*, 115203.

[24] a) W.-Q. Deng, W. A. Goddard, *J. Phy. Chem. B* **2004**, *108*, 8614; b) S.-H. Wen, A. Li, J. Song, W.-Q. Deng, K.-L. Han, W. A. Goddard, *J. Phy. Chem. B* **2009**, *113*, 8813.

[25] J. Jortner, *J. Chem. Phys.* **1976**, *64*, 4860; b) S. H. Lin, C. H. Chang, K. K. Liang, R. Chang, Y. J. Shiu, J. M. Zhang, T. S. Yang, M. Hayashi, F. C. Hsu, *Adv. Chem. Phys.* **2002**, *121*, 1.

[26] a) K. Senthilkumar, F. C. Grozema, F. M. Bickelhaupt, L. D. A. Siebbelesb, *J. Chem. Phys.* **2003**, *119*, 9809; b) G. Te Velde, F. M. Bickelhaupt, E. J. Baerends, C. Fonseca Guerra, S. J. A. Van Gisbergen, J. G. Snijders, T. Ziegler, *J. Comput. Chem.* **2001**, *22*, 931.

[27] R. Li, J. W. Ward, D.-M. Smilgies, M. M. Payne, J. E. Anthony, O. D. Jurchescu, A. Amassian, *Adv. Mater.* **2012**, *24*, 5553.

[28] S. S. Lee, C. S. Kim, E. D. Gomez, B. Purushothaman, M. F. Toney, C. Wang, A. Hexemer, J. E. Anthony, Y.-L. Loo, *Adv. Mater.* **2009**, *21*, 3605.